Synsint Research Group

Available online at www.synsint.com

Synthesis and Sintering

ISSN 2564-0186 (Print), **ISSN** 2564-0194 (Online)

Research article

High-temperature spark plasma sintering of h-BN composites reinforced with carbon nanotubes, carbon fibers, and graphene nanoplates

Hossein Eslami-Shahed [a], Khanali Nekouee [a,*], Farhad Moravvej-Farshi [a], Fatemeh Dabir [b]

[a] *Faculty of Materials and Manufacturing Technologies, Malek Ashtar University of Technology, Tehran, 1491912354, Iran*
[b] *Non-Metallic Materials Research Group, Niroo Research Institute (NRI), Tehran, 14686-13113, Iran*

ABSTRACT

In this study, two h-BN-based composites reinforced with carbon fibers (CF) and carbon fibers/carbon nanotubes (CNTs)/graphene nanoplates (GNPs) have been produced successfully through a high-temperature spark plasma sintering. 1 wt% short carbon fibers (length of 5 mm) with 0.1 wt% of CNTs and also 0.1 wt% of GNPs as hybrid composite were mixed through a simple mixing method including a high energy sonicating and stirring on the hot plate in ethanol media until drying. Moreover, the h-BN/1 wt% CF composite was mixed with a similar method to compare the impacts of CNTs and GNPs addition on the mechanical properties and microstructure of the h-BN/CF composite. The high-temperature spark plasma sintering processes were performed at vacuum conditions of almost 20–25 MPa with a starting pressure of 10 and a final applied pressure of 50 MPa at a maximum temperature of 1900 °C. Both prepared samples showed near full densification of higher than 98.1% of the theoretical density determined by Archimedes' principle. Investigation of the crystalline phases by XRD represented only related peaks to h-BN. The FESEM images indicated an almost uniform distribution of reinforcement in the h-BN matrix. Furthermore, the polished surface of the provided samples showed only the pulled-out carbon fibers effects while the fracture surfaces confirmed the presence of CF and its tunneling effects. The obtained mechanical properties revealed 273±12 MPa of bending strength, 1.32±0.1 GPa of Vickers hardness, and 4.79±0.2 MPa.m$^{0.5}$ fracture toughness for the prepared hybrid composite.

KEYWORDS

Hexagonal boron nitride
CNTs
Carbon fiber
GNPs
Spark plasma sintering

OPEN ACCESS

1. Introduction

Hexagonal boron nitride (h-BN), commonly called as "white graphene," because of some similar lamellar structure has been considered adequately owing to its outstanding chemical and physical features like friction coefficient and low density, non-wetting characteristics, chemical and thermal inertness, oxidation, and chemical resistance [1–4]. Consequently, BN and BN-comprising composites have significant applications in many fields, including industries dealing with the melting of metals, aerospace, and many chemical engineering applications [5–8]. The lamellar structure of h-BN forms as a result of the strong covalent bonds (sp^2 bonds between N and B atoms in the layers) and the weak forces of van der Waals between layers [9–11].

The dense form of h-BN materials with many applications in high-temperature industries has difficulties in production due to its sintering problems [12, 13]. Strong covalent bonding, point low diffusion coefficients, and also high melting in h-BN ceramics lead to the

---

* Corresponding author. *E-mail address:* khnekouee@gmail.com (K. Nekouee)

Received 7 November 2024; Received in revised form 8 December 2024; Accepted 15 December 2024.

https://doi.org/10.53063/synsint.2024.44261

prevention of movement of the grains; Moreover, the anisotropic growth of layers can remain pores which makes the h-BN hard to produce in the dense form with proper mechanical properties [14–16]. To overcome this problem some research focused on using sintering aids such as MAS (MgO-Al_2O_3-SiO_2) [17] glass-ceramics, Y_2O_3-Al_2O_3-SiO_2 [18], MgAlON [19] and other popular sintering additives in high-temperature ceramics [20–22]. One of the unique solutions for the sintering problem of h-BN-based ceramic is the novel sintering process like the spark plasma sintering process which can produce most ceramic materials with high melting points even in pure form and proper properties [23–26].

Spark plasma sintering has been utilized, as a suitable technique, to fabricate various materials without considering their melting point and related problems in sintering and densification [27–30]. The advantages like controlled atmosphere, fast heating rate, applied pressure, sparks, and plasma condition, etc. make this method a promising candidate for preparing dense ceramic materials without any sintering additives normally used to enhance the densification based on liquid phase sintering [31–35]. To reach the proper densification of additive-free h-BN bulk ceramic material, a pressure-assisted sintering method is essential. Spark plasma sintering offers the production of h-BN-based ceramic material with proper densification based on literature reviews [36–39].

The weak mechanical characteristics of bulk h-BN ceramics are improved by utilizing different reinforcements such as hard ceramics [40], carbon-based phases [41], or even metallic phases that produce reaction products as composite materials [42, 43]. Although sintering aids reduce the sintering temperature, they also reduce the working temperature of the produced part. For example, boron oxide with a very low melting temperature or silicon oxide with a low melting temperature compared to boron nitride, if present in the final part under high-temperature working conditions, will lead to local melting and the part not functioning properly. On the other hand, although using hard reinforcing particles with a very high melting temperature can improve the final properties, this occurs when maximum densification is achieved. As a result, due to the prevention of high densification and the remaining porosity in the system, these hard particles do not improve the mechanical properties and lead to weakening. Therefore, in this work, the impact of carbon fibers, CNTs, and GNPs was investigated on the mechanical characteristics of h-BN-based ceramic composites as single and hybrid reinforcements. To the best of the authors' knowledge, adding carbon fibers, GNPs, and CNTs to the h-BN materials was done to enhance the thermal conductivity of the final products [44–48]. It seems that there is no similar research to investigate the influence of carbon-based material as reinforcement phases on the mechanical characteristics of high-temperature spark plasma sintered h-BN-based composite.

2. Experimental procedures

The h-BN powders were synthesized by heating a mixture of commercial urea and boric acid (99% purity) in a nitrogen atmosphere. The synthesis process was implemented based on the authors' previous work [3]. The mentioned synthesized h-BN powders with 1 wt% carbon fibers (average diameter of 5 µm, length of 5 mm, China), 0.1 wt% of CNTs (MWCNTs, >95% purity, OD: 5–15 nm, US Research nanomaterials Inc.) and 0.1 wt% of GNPs (average thickness ~ 2 nm, particle diameter < 2 µm, mean surface area: 750 m^2/g, XG Sciences, Grade C) were added into 100 ml ethanol containing 0.01 g sodium dodecyl benzene sulfonate (SDS) and ultra-sonicated for 20 min to unwarp agglomeration of carbon-based phases. Similarly, the other batch containing h-BN powders and 1 wt% carbon fibers was poured into 100 ml ethanol. After that, both mixtures were dried on a stirring hot plate while stirring at a temperature of 70 °C. The obtained mixtures of two composites were directly placed in a mold made of graphite covered by graphite foil (30 mm diameter). The sintering process was carried out by SPS apparatus (SPS-20T-10, Easy Fashion Industry, China) under vacuum conditions (20–25 MPa) and at a maximum sintering temperature of 1900 °C. The pressures applied at the beginning and end of the process were 10 MPa and 50 MPa, respectively. The external load increased during the holding period at the elevated temperature of 1900 °C. Fig. 1 explains a summary of the

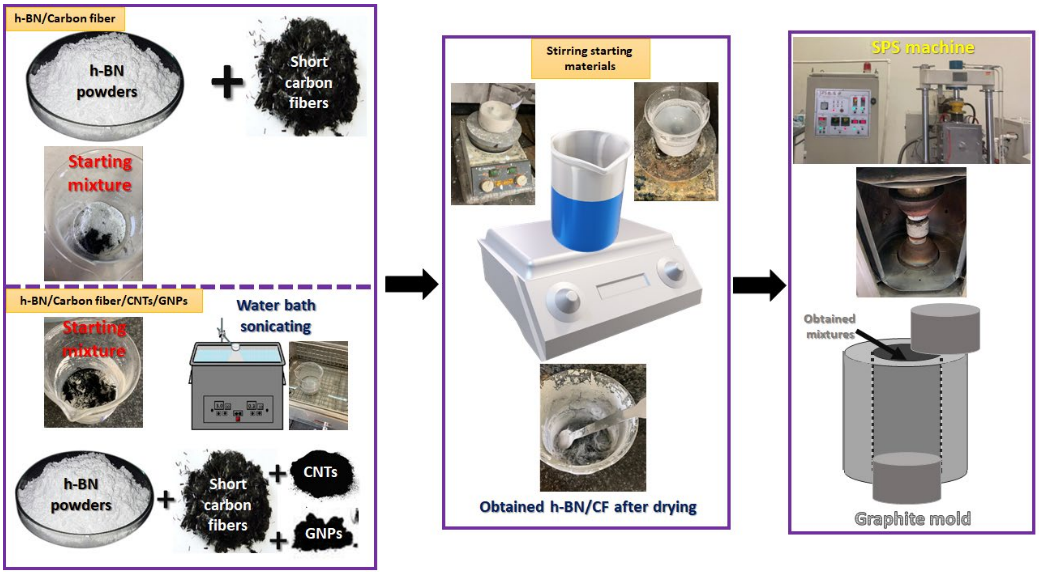

Fig. 1. Summary of preparation method including schematics and camera pictures.

preparation method including schematic and camera pictures. After completing the sintering process, the graphite foils were removed from the sample surfaces through grinding, and three bar-shaped specimens (25×5×5 mm) were cut from the resulting cylindrical samples.

The Archimedes principle was utilized to compute the relative density of the provided specimens. To identify crystalline phases and also evaluate the microstructure of samples, XRD (Philips, X-Pert System, Cu k_α radiation, 2θ of 10–80 °) and FESEM (MIRA 3 TESCAN, Czech Republic) equipped with EDS techniques were utilized, respectively. The flexural strength of samples was measured through a three-point bending strength test (Santam-STm20 Iran). A Vickers microhardness test was performed at room temperature using an MKV-h21 microhardness tester, with a load of 1 kgf and a holding time of 10 seconds. The results were obtained by calculating the average of 10 successful indentations. The measurement of crack lengths was also used for estimating indentation fracture toughness (K_{IC}) based on Evans' equation [49] as follows:

$$K_{IC} = 0.16\ Hv.a^{2}.c^{-3/2} \tag{1}$$

where Hv, a, and c show Vickers hardness, half the mean diagonal length of the Vickers indentation, and the average length of the cracks obtained from the indentation, respectively. The values of a and c were measured using FESEM.

3. Results and discussion

Fig. 2 displays the changes in punch movement, displacement rate, and temperature versus time obtained from the SPS procedure of two investigated composites as h-BN/CF and h-BN/CF/CNT/GNP specimens. These types of curves have become as useful tools to monitor the sintering process and especially are useful methods for readers to repeat the sintering procedures in detail. Regarding the Fig. 2, almost a similar heating regime was chosen for both samples and after 28 min the temperature was raised to 1900 °C. By increasing temperature until nearly 1500 °C no obvious changes were detected in the punch displacement which is expected due to the nature of composites' components (carbon and h-BN) considered as high melting point materials. The first stage of sintering for both the prepared composites started at the above-mentioned temperature and by increasing temperature, the punch displacement increased slowly. By reaching a temperature of almost 1800–1850 °C, the 2nd stage of densification and somehow the original stage of the sintering process in terms of densification occurred. After that, the applied load was progressively increased from 10 to 50 MPa at a temperature of 1900 °C which led to a dominant stage in densification. Regarding Fig. 2, 35 min into the sintering process and during its last stage, no significant changes in punch displacement were observed, indicating that the process had achieved maximum densification under the applied temperature and pressure conditions. Moreover, the total shrinkage of the h-BN/CF/CNT/GNP hybrid composite (punch displacement change) is lower than the h-BN/CF specimen that appears to be associated with the formation of GNPs and/or CNTs agglomerates and prevents proper densification.

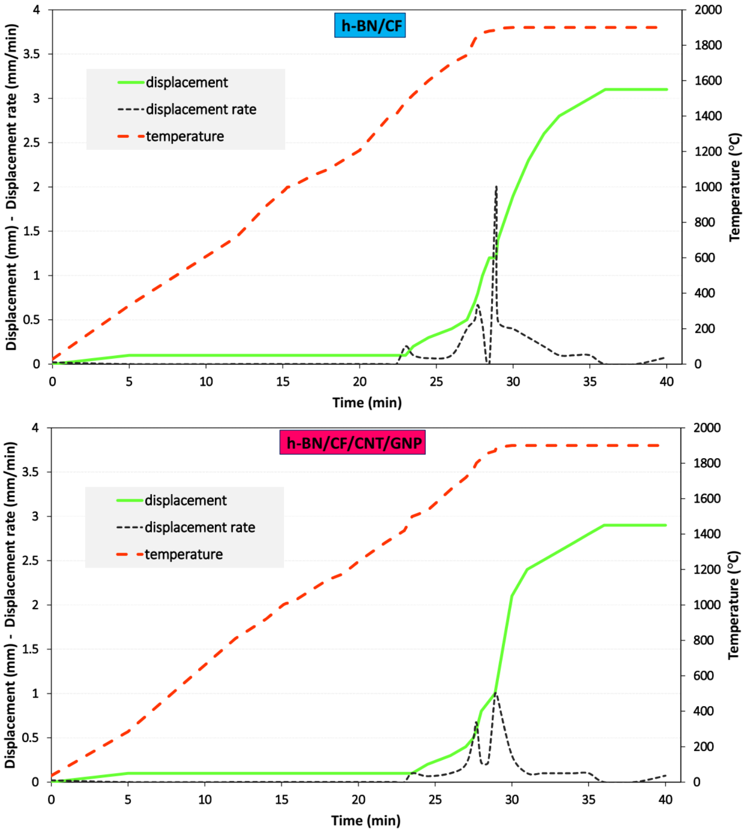

Fig. 2. Curves of punch displacement-temperature-time attained from the SPS of composites.

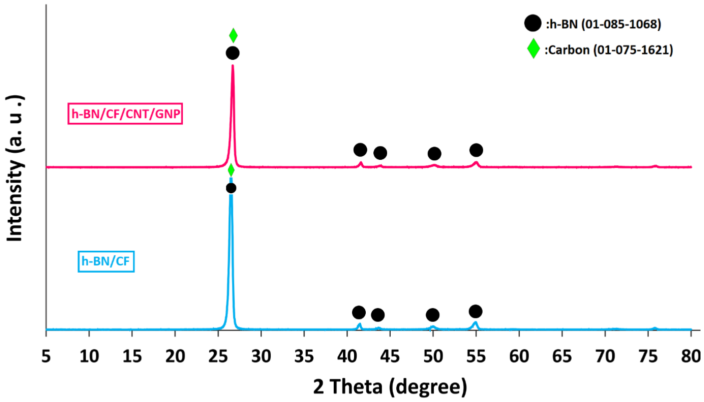

Fig. 3. XRD patterns of h-BN/CF and h-BN/CF-CNT-GNP hybrid composites.

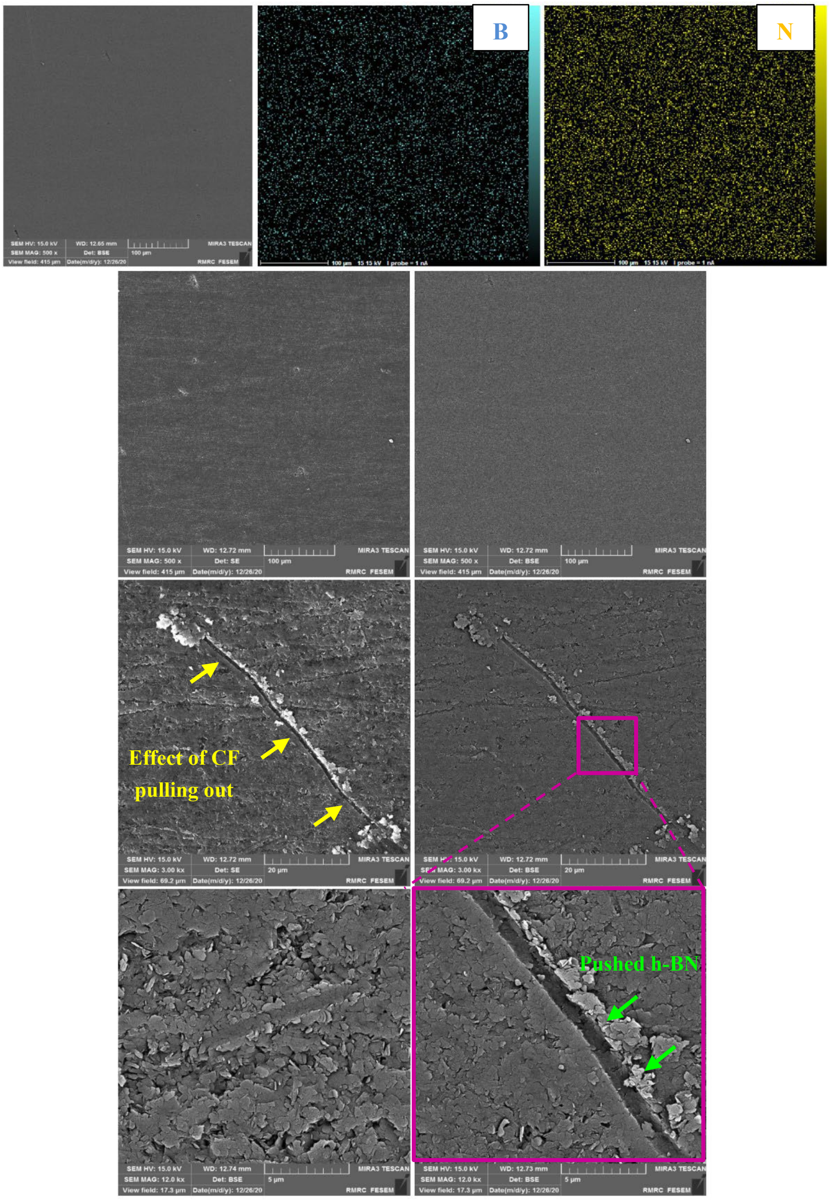

Fig. 4. FESEM images from the polished surface of h-BN/CF composite along with corresponding EDS elemental map.

Fig. 3 shows XRD patterns related to the h-BN/CF and h-BN/CF/CNT/GNP composite materials from the polished surface which is perpendicular to the punch axis. As it is clear from Fig. 3, the prominent peaks in the both of obtained patterns are related to the h-BN as a crystalline phase. Moreover, there is an overlapping of the carbon peak and the related peak to the h-BN at around 2θ=26 °. Moreover, as anticipated, there is no indication of a reaction between h-BN and carbon phases based on XRD detection's limit.

Fig. 4 depicts FESEM images and relevant EDS elemental mapping of the polished surface of the h-BN/CF composite, including insets at higher magnifications. Regarding Fig. 4, the EDS elemental mapping of the h-BN/CF composite surface at low magnification (BSE and SE modes) demonstrates the presence of nitrogen and boron atoms throughout the surface, verifying that h-BN remains stable without undergoing decomposition or reaction. As shown in Fig. 4, no carbon fibers were detected; however, the effects of their pull-out due to the polishing process were clearly observed. Moreover, it seems that the bonding between h-BN and carbon fibers after detachment leads to pushing the h-BN planes on the surface in the same direction as the remaining pushing lines.

FESEM images from the fracture surface of the h-BN/CF composite with EDS spectra and quantitative analyses are shown in Fig. 5. Considering Fig. 5, carbon fibers are easily visible on the fracture surface of the sample. Moreover, it seems that carbon fibers have a strong attachment to the BN matrix which has been covered by h-BN particles after fracture. A strong interface between the reinforcement and the matrix in the composite is essential for effective load transfer to the reinforcement phase and enhancement of composite mechanical properties. The quantitative analysis from α and β spots in Fig. 5, can confirm the matrix is h-BN while the amount of carbon is high at the spot α which approves the presence of carbon fiber. The high aspect ratio of CFs, as seen in Fig. 5, allows them to bridge cracks effectively and bear tensile loads, which helps in transferring stress across crack surfaces.

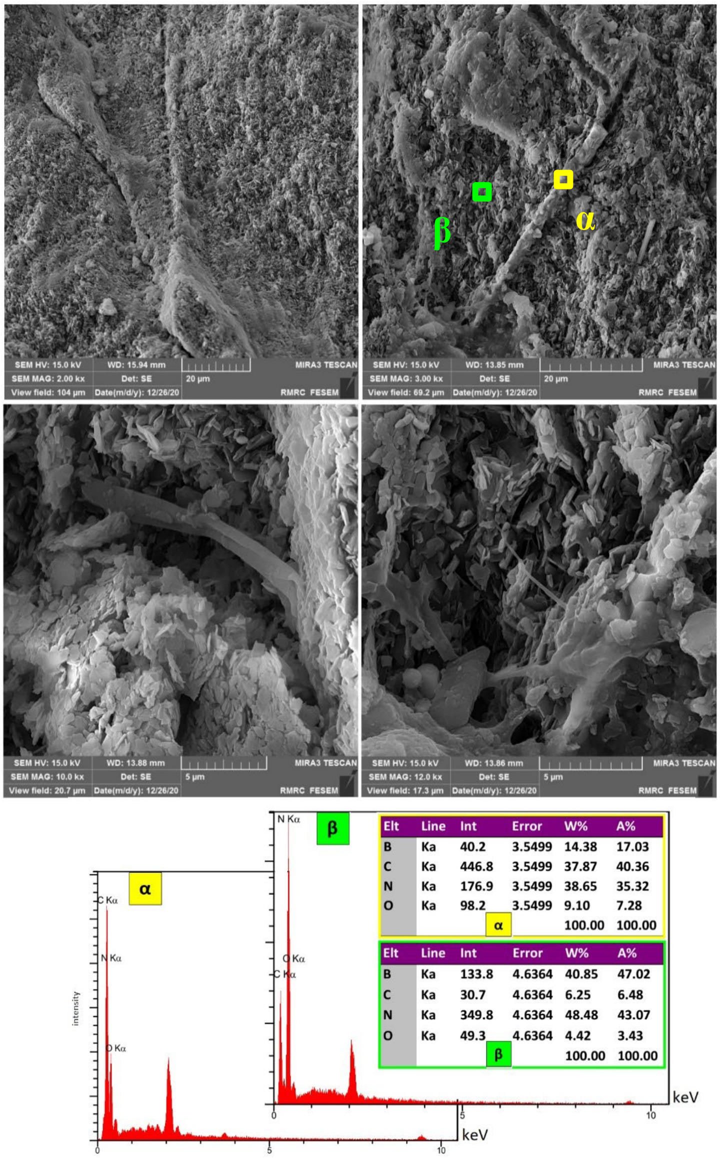

Elt	Line	Int	Error	W%	A%
B	Ka	40.2	3.5499	14.38	17.03
C	Ka	446.8	3.5499	37.87	40.36
N	Ka	176.9	3.5499	38.65	35.32
O	Ka	98.2	3.5499	9.10	7.28
		α		100.00	100.00

Elt	Line	Int	Error	W%	A%
B	Ka	133.8	4.6364	40.85	47.02
C	Ka	30.7	4.6364	6.25	6.48
N	Ka	349.8	4.6364	48.48	43.07
O	Ka	49.3	4.6364	4.42	3.43
		β		100.00	100.00

Fig. 5. FESEM images, EDS spectra, and quantitative analyses of h-BN/CF composite fracture surface.

Fig. 6 reveals FESEM images of h-BN/CF/CNT/GNP hybrid composite at different magnifications. Regarding Fig. 6, the effect of carbon fiber as a result of fiber pulling out was seen as well as the polished surface of the h-BN/CF composite. It is observed that the microstructure of the sample does not show any pores and porosities at the composite surface. Because CNTs are almost undetectable on the polished surface of the composite, but in the highest magnification images belonging to Fig. 6, a mixture of CNTs agglomeration with h-BN particles can be seen.

Fig. 7 illustrates FESEM images of the fracture surface of h-BN/CF/CNT/GNP hybrid composite from ultra-low to high magnifications through insets on them. As can be seen from Fig. 7, the carbon fibers at the fracture surface were detected while some tunneling can be found as a result of carbon pulling out. Also, some fibers were covered by the BN particles which seems due to good attachment between CF and h-BN. Moreover, the high magnification images in Fig. 7 reveal that CNTs and GNPs with CF reinforcement led to the forming of a hybrid composite. It is worth noting that distinguishing GNPs in the lamellar structure of h-BN is too hard but the prepared image shows a transparent plane that can considered as graphene. Fig. 7 also shows the carbon fiber rupture which can occur as a result of a perfect attachment between h-BN and CF during fracture. The combined effect of CFs, CNTs, and GNPs with varying aspect ratios and different morphologies optimizes the mechanical features of the h-BN ceramic composite. The high aspect ratios of CFs and CNTs effectively bridge and arrest cracks, while the planar GNPs inhibit crack propagation.

Table 1 summarizes the mechanical properties and relative density calculation of h-BN/CF and h-BN/CF/CNT/GNP composites including Vickers hardness, fracture toughness, and flexural strength. Considering Table 1, both prepared composites have near fully dense relative density compared to the other prepared h-BN-based ceramic in the literature reviews. The Vickers hardness of the hybrid composite is a little higher than the h-BN/CF composite which by considering the calculated standard deviation seems that the attained Vickers hardness of samples is in the same range. In the case of flexural strength and fracture toughness, the hybrid prepared composite shows a higher amount which is expected as the original goal of this work.

Fig. 8 indicates the curves of load-extension achieved from a test of the three-point bending strength of both sintered composites. Regarding Fig. 8, the fracture load and extension of the hybrid composite are higher compared to the composite containing only carbon fiber as reinforcement. Notably, the area beneath the load-extension curve can serve as an indicator of toughness (adsorb energy until fracture). Therefore, considering Fig. 8 the area under the load-extension curve relating to the h-BN/CF/CNT/GNP sample is higher than the h-BN/CF composite which is fully consistent with the fracture toughness calculated in Table 1.

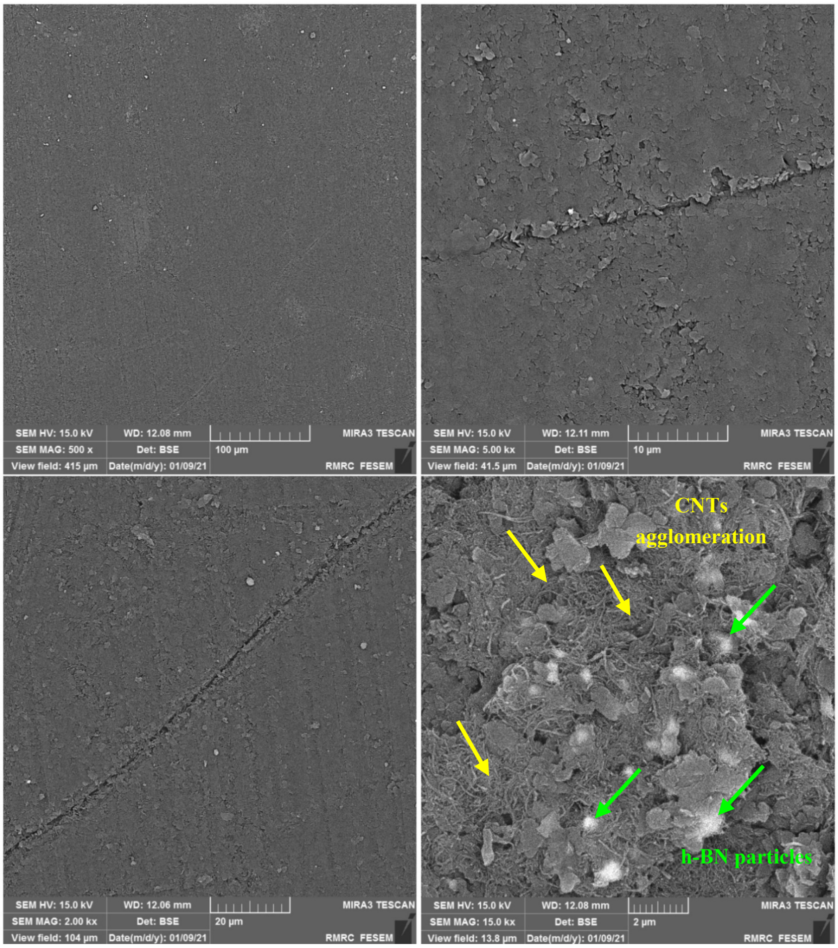

Fig. 6. FESEM images of h-BN/CF/CNT/GNP hybrid composite polished surface.

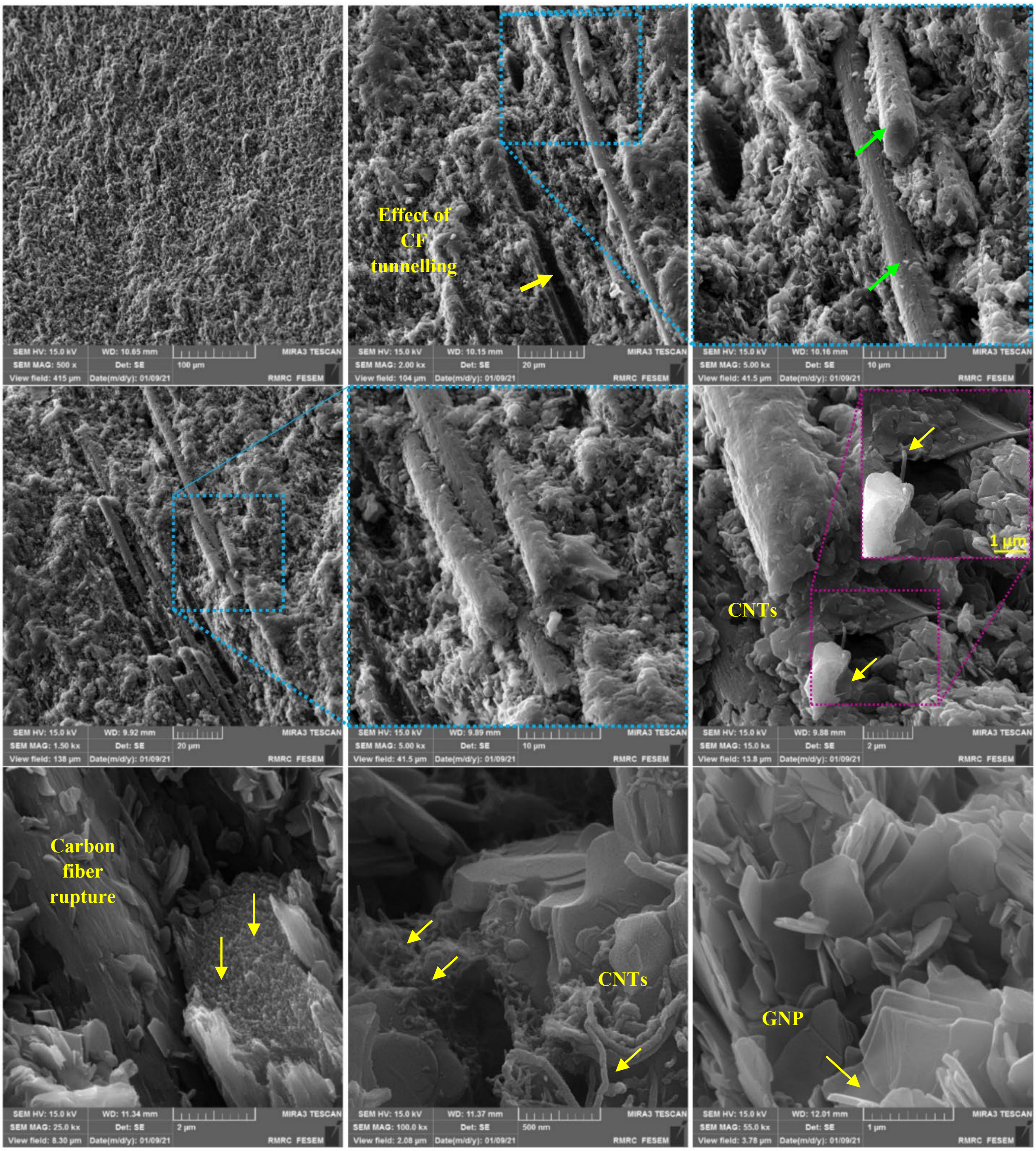

Fig. 7. FESEM images of h-BN/CF/CNT/GNP hybrid composite fracture surface from low to high magnifications.

Table 1. Mechanical properties and relative density of SPSed h-BN-based composites.

Composites	Relative density (%)	Vickers hardness (GPa)	Flexural strength (MPa)	Fracture toughness ($MPa.m^{1/2}$)
h-BN/CF	98.69±0.21	1.19±0.08	206±13	3.84±0.16
h-BN/CF/CNT/GNP	98.17±0.25	1.32±0.1	273±12	4.79±0.2

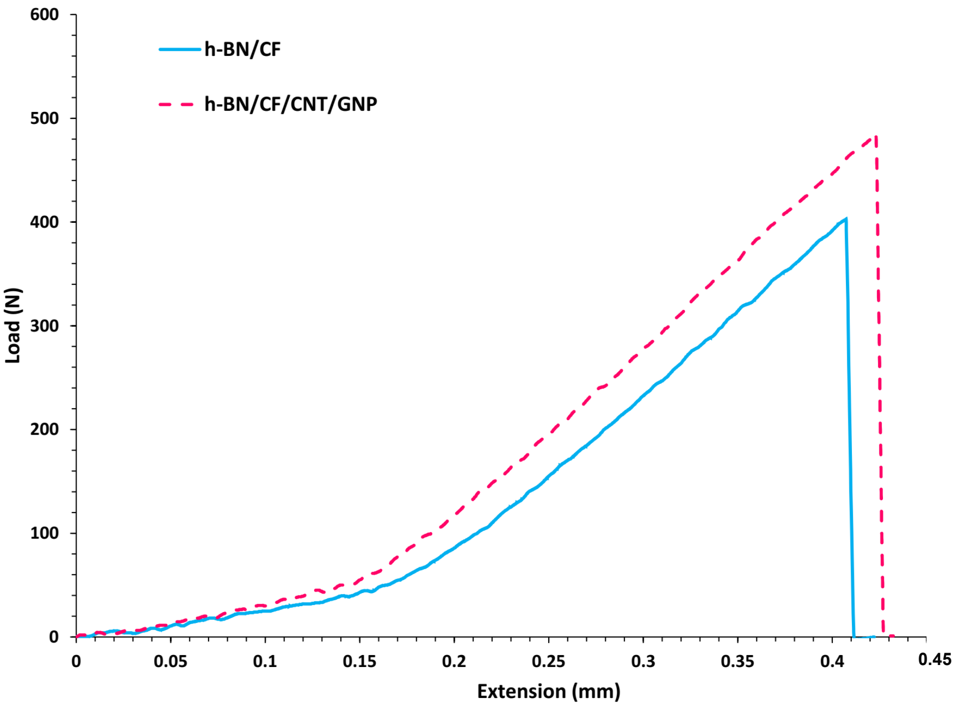

Fig. 8. Curves of load-extension during bending strength test of prepared composites.

4. Conclusions

Two h-BN-based ceramics reinforced with carbon fibers and carbon fiber-CNTs-GNPs were successfully fabricated as conventional and hybrid composites by a high-temperature spark plasma sintering process. Both prepared composites were sintered at 1900 °C and the results indicated that there is no sign of decomposition and/or reaction of components of composites. The microstructural investigations on the polished surface of samples revealed the effects of CF on the surface as a result of the pulling-out phenomenon and polishing process. The fracture surface of both prepared composites exhibited carbon fibers with a weak and strong attachment to the h-BN matrix which after fracture led to formation tunnels, pulled out, and ruptures. The obtained mechanical properties indicated that adding 0.1 wt% of CNTs and GNPs led to an increase in fracture toughness from 3.84 to 4.79 MPa.m$^{1/2}$, flexural strength from 206 to 273 MPa, and Vickers hardness from 1.19 to 1.32 GPa compared to the h-BN/1 wt% CF composite.

CRediT authorship contribution statement

Hossein Eslami-Shahed: Conceptualization, Investigation, Writing-original draft, Writing-review & editing.

Khanali Nekouee: Project administration, Funding acquisition, Conceptualization, Writing-original draft, Writing-review & editing, visualization, Visualization, Data curation.

Farhad Moravej-Farshi: Writing-original draft, Writing-review & editing, visualization, Visualization, Data curation.

Fatemeh Dabir: Writing-original draft, Writing-review & editing, visualization, Visualization, Data curation.

Data availability

The data underlying this article will be shared on reasonable request to the corresponding author.

Declaration of competing interest

The authors declare no conflict of interest; the authors declare that they have no known competing financial interests or personal relationships that could have appeared to influence the work reported in this paper.

Funding and acknowledgment

This research did not receive any specific grant from funding agencies in the public, commercial, or not-for-profit sectors.

References

[1] D. Cai, Z. Yang, X. Duan, P. He, S. Wang, et al., Inhibiting crystallization mechanism of h-BN on α-cordierite in BN-MAS composites, J. Eur. Ceram. Soc. 36 (2016) 905–909. https://doi.org/10.1016/j.jeurceramsoc.2015.10.007.

[2] M. Hubácek, M. Ueki, Effect of the Orientation of Boron Nitride Grains on the Physical Properties of Hot-Pressed Ceramics, J. Am. Ceram. Soc. 82 (1999) 156–160. https://doi.org/10.1111/j.1151-2916.1999.tb01735.x.

[3] H. Eslami-shahed, N. Ehsani, The effects of adding CNTs and GNPs on the microstructure and mechanical properties of hexagonal-boron nitride, Ceram. Int. 46 (2020) 22005–22014. https://doi.org/10.1016/j.ceramint.2020.05.176.

[4] J. Men, B. Li, J. Li, G. Li, J. Chen, X. Hou, Amorphous liquid phase induced synthesis of boron nitride nanospheres for improving

sintering property of h-BN/ZrO2 composites, Ceram. Int. 46 (2020) 8031–8038. https://doi.org/10.1016/j.ceramint.2019.12.027.

[5] J. Eichler, C. Lesniak, Boron nitride (BN) and BN composites for high-temperature applications, J. Eur. Ceram. Soc. 28 (2008) 1105–1109. https://doi.org/10.1016/j.jeurceramsoc.2007.09.005.

[6] C. Steinborn, M. Herrmann, U. Keitel, A. Schönecker, J. Räthel, et al., Correlation between microstructure and electrical resistivity of hexagonal boron nitride ceramics, J. Eur. Ceram. Soc. 33 (2013) 1225–1235. https://doi.org/10.1016/j.jeurceramsoc.2012.11.024.

[7] D. Cai, Z. Yang, X. Duan, B. Liang, Q. Li, et al., A novel BN–MAS system composite ceramics with greatly improved mechanical properties prepared by low temperature hot-pressing, Mater. Sci. Eng: A. 633 (2015) 194–199. https://doi.org/10.1016/j.msea.2015.03.030.

[8] D. Wei, Q. Meng, D. Jia, Microstructure of hot-pressed h-BN/Si3N4 ceramic composites with Y2O3–Al2O3 sintering additive, Ceram. Int. 33 (2007) 221–226. https://doi.org/10.1016/j.ceramint.2005.09.004.

[9] H. Qin, Y. Liang, J. Huang, Size and temperature effect on the mechanical properties of graphene/hexagonal boron nitride van der Waals heterostructure, Mater. Sci. Eng: B. 265 (2021) 115006. https://doi.org/10.1016/j.mseb.2020.115006.

[10] A.P. Barboza, A.C. Souza, M.J. Matos, J.C. Brant, T.C. Barbosa, et al., Graphene/h-BN heterostructures under pressure: From van der Waals to covalent, Carbon. 155 (2019) 108–113. https://doi.org/10.1016/j.carbon.2019.08.054.

[11] A. Acharya, S. Sharma, X. Liu, D. Zhang, Y.K. Yap, A Review on van der Waals Boron Nitride Quantum Dots, C. 7 (2021) 35. https://doi.org/10.3390/c7020035.

[12] X. Duan, M. Wang, D. Jia, N. Jing, Z. Wu, et al., Anisotropic mechanical properties and fracture mechanisms of textured h-BN composite ceramics, Mater. Sci. Eng: A. 607 (2014) 38–43. https://doi.org/10.1016/j.msea.2014.03.132.

[13] X. Duan, D. Jia, Z. Wu, Z. Tian, Z. Yang, et al., Effect of sintering pressure on the texture of hot-press sintered hexagonal boron nitride composite ceramics, Scr. Mater. 68 (2013) 104–107. https://doi.org/10.1016/j.scriptamat.2012.09.012.

[14] Y. Zhao, Y. Zhang, H. Gong, X. Wang, H. Sun, Effects of Y2O3–MgO nanopowders content on mechanical and dielectric properties of porous BN/Si3N4 composites, Ceram. Int. 41 (2015) 3618–3623. https://doi.org/10.1016/j.ceramint.2014.11.025.

[15] M.I. Litter, A. Ahmad, Industrial Applications of Nanoparticles A Prospective Overview, CRC Press: Boca Raton, FL, USA. (2023). https://doi.org/10.1201/9781003183525.

[16] D. Jia, L. Zhou, Z. Yang, X. Duan, Y. Zhou, Effect of preforming process and starting fused SiO2 particle size on microstructure and mechanical properties of pressurelessly sintered BNp/SiO2 ceramic composites, J. Am. Ceram. Soc. 94 (2011) 3552–3560. https://doi.org/10.1111/j.1551-2916.2011.04540.x.

[17] B. Niu, D. Cai, Z. Yang, X. Duan, W. Duan, et al., Effects of sintering temperature on the microstructure and properties of h-BN ceramics with MAS as liquid sintering aid, Ceram. Int. 46 (2020) 1076–1082. https://doi.org/10.1016/j.ceramint.2019.09.074.

[18] Z. Zhang, X. Duan, B. Qiu, Z. Yang, D. Cai, et al., Anisotropic properties of textured h-BN matrix ceramics prepared using 3Y2O3-5Al2O3 (-4MgO) as sintering additives, J. Eur. Ceram. Soc. 39 (2019) 1788–1795. https://doi.org/10.1016/j.jeurceramsoc.2019.01.003.

[19] Z. Zhang, L. Teng, W. Li, Mechanical properties and microstructures of hot-pressed MgAlON–BN composites, J. Eur. Ceram. Soc. 27 (2007) 319–326. https://doi.org/10.1016/j.jeurceramsoc.2006.04.184.

[20] T. Hagio, H. Yoshida, Sintering and crystallization of ground hexagonal boron nitride powders, J. Mater. Sci. Let. 13 (1994) 653–655. https://doi.org/10.1007/BF00271224.

[21] X.J. Gao, D.M. Yan, J.W. Cao, C. Zhang, X.M. Mu, et al., The study on the property and the microstructure of pressureless sintered h-BN ceramics, Adv. Mater. Res. 1104 (2015) 9–14. https://doi.org/10.4028/www.scientific.net/AMR.1104.9.

[22] H. Yang, H. Fang, H. Yu, Y. Chen, L. Wang, et al., Low temperature self-densification of high strength bulk hexagonal boron nitride, Nat. Commun. 10 (2019) 854. https://doi.org/10.1038/s41467-019-08580-9.

[23] E. Ghasali, M. Alizadeh, A.H. Pakseresht, T. Ebadzadeh, Preparation of silicon carbide/carbon fiber composites through high-temperature spark plasma sintering, J. Asian Ceram. Soc. 5 (2017) 472–478. https://doi.org/10.1016/j.jascer.2017.10.004.

[24] E. Ghasali, K. Shirvanimoghaddam, M. Alizadeh, T. Ebadzadeh, Ultra-low temperature fabrication of vanadium carbide reinforced aluminum nano composite through spark plasma sintering, J. Alloys Compd. 753 (2018) 433–445. https://doi.org/10.1016/j.jallcom.2018.04.239.

[25] E. Ghasali, Y. Palizdar, A. Jam, H. Rajaei, T. Ebadzadeh, Effect of Al and Mo addition on phase formation, mechanical and microstructure properties of spark plasma sintered iron alloy, Mater. Today Commun. 13 (2017) 221–231. https://doi.org/10.1016/j.mtcomm.2017.10.005.

[26] E. Ghasali, Y. Orooji, A. Faeghi-nia, M. Alizadeh, T. Ebadzadeh, Characterization of mullite-Nd2O3 composite prepared through spark plasma sintering, Ceram. Int. 47 (2021) 16200–16207. https://doi.org/10.1016/j.ceramint.2021.02.198.

[27] M. Vukšić, I. Žmak, L. Ćurković, A. Kocjan, Spark plasma sintering of dense alumina ceramics from industrial waste scraps, Open Ceram. 5 (2021) 100076. https://doi.org/10.1016/j.oceram.2021.100076.

[28] U.C. Oliver, A.V. Sunday, E.I.-E.I. Christain, M.M. Elizabeth, Spark plasma sintering of aluminium composites—a review, Int. J. Adv. Manuf. Technol. 112 (2021) 1819–1839. https://doi.org/10.1007/s00170-020-06480-7.

[29] Z.-Y. Hu, Z.-H. Zhang, X.-W. Cheng, F.-C. Wang, Y.-F. Zhang, S.-L. Li, A review of multi-physical fields induced phenomena and effects in spark plasma sintering: Fundamentals and applications, Mater. Design. 191 (2020) 108662. https://doi.org/10.1016/j.matdes.2020.108662.

[30] Z. Yılmaz, N. Ay, The investigation of synthesis and textured properties of in situ formed hBN with spark plasma sintering, Mater. Chem. Phys. 316 (2024) 129043. https://doi.org/10.1016/j.matchemphys.2024.129043.

[31] R. Chaim, Densification mechanisms in spark plasma sintering of nanocrystalline ceramics, Mater. Sci. Eng: A. 443 (2007) 25–32. https://doi.org/10.1016/j.msea.2006.07.092.

[32] O.J. Akinribide, B.A. Obadele, O.O. Ayeleru, S. Akinwamide, K. Nomoto, et al., The role of graphite addition on spark plasma sintered titanium nitride, J. Mater. Res. Technol. 9 (2020) 6268–6277. https://doi.org/10.1016/j.jmrt.2020.03.040.

[33] O. Ogunbiyi, T. Jamiru, E. Sadiku, O. Adesina, L. Beneke, T.A. Adegbola, Spark plasma sintering of nickel and nickel based alloys: A Review, Procedia Manuf. 35 (2019) 1324–1329. https://doi.org/10.1016/j.promfg.2019.05.022.

[34] E. Ghasali, T. Ebadzadeh, M. Alizadeh, M. Razavi, Unexpected SiC nanowires growth during spark plasma sintering of WC-10Si: a comparative study on phase formation and microstructure properties against WC-10Co cermet, J. Alloys Compd. 786 (2019) 938–952. https://doi.org/10.1016/j.jallcom.2019.02.059.

[35] H. Wang, Y. Zeng, Y. Dai, Y. Li, T. Zhu, Z. Fu, Enhanced mechanical properties of boron carbide ceramics prepared by spark plasma sintering with boron nitride nanosheets addition, J. Eur. Ceram. Soc. 44 (2024) 116735. https://doi.org/10.1016/j.jeurceramsoc.2024.116735.

[36] F.R. Zhai, M. Lu, K. Shan, Z.Z. Yi, Z.P. Xie, Spark plasma sintering and characterization of mixed h-bn powders with different grain sizes, Solid State Phenom. 281 (2018) 414–419. https://doi.org/10.4028/www.scientific.net/SSP.281.414.

[37] T.F. Almeida, M.P. Gonçalves, R.H.G.A. Kiminami, Microstructure and dielectric properties of hexagonal boron nitride prepared by hot pressing (uniaxial and isostatic) and by spark plasma sintering, Adv.

Appl. Ceram. 119 (2020) 41–48. https://doi.org/10.1080/17436753.2019.1689704.

[38] M. Ehsani, M. Zakeri, M. Razavi, The effect of temperature on the physical and mechanical properties of nanostructured boron nitride by spark plasma sintering, J. Alloys Compd. 835 (2020) 155317. https://doi.org/10.1016/j.jallcom.2020.155317.

[39] Y. Wu, Y. Zhang, X. Wang, W. Hu, S. Zhao, et al., Twisted-layer boron nitride ceramic with high deformability and strength, Nature. 626 (2024) 779–784. https://doi.org/10.1038/s41586-024-07036-5.

[40] Q. Guo, J. Wang, J. Pei, J. Li, L. Zhang, Effect of SiC Content on the Microstructure and Properties of Zr2Al4C5/SiC Composites in situ Fabricated by Spark Plasma Sintering, IOP Conference Series: Materials Science and Engineering, IOP Publishing. 678 (2019) 012073. https://doi.org/10.1088/1757-899X/678/1/012073.

[41] C. Xia, A.C. Garcia, S.Q. Shi, Y. Qiu, N. Warner, et al., Hybrid boron nitride-natural fiber composites for enhanced thermal conductivity, Sci. Rep. 6 (2016) 34726. https://doi.org/10.1038/srep34726.

[42] Y. Yuan, X. Cheng, R. Chang, T. Li, J. Zang, et al., Reactive sintering cBN-Ti-Al composites by spark plasma sintering, Diam. Relat. Mater. 69 (2016) 138–143. https://doi.org/10.1016/j.diamond.2016.08.009.

[43] B. Wang, Y. Qin, F. Jin, J.-F. Yang, K. Ishizaki, Pulse electric current sintering of cubic boron nitride/tungsten carbide–cobalt (cBN/WC–Co) composites: effect of cBN particle size and volume fraction on their microstructure and properties, Mater. Sci. Eng: A. 607 (2014) 490–497. https://doi.org/10.1016/j.msea.2014.04.029.

[44] Z. Su, H. Wang, X. Ye, K. Tian, W. Huang, et al., Enhanced thermal conductivity of functionalized-graphene/boron nitride flexible laminated composite adhesive via a facile latex approach, Compos. A: Appl. Sci. Manuf. 99 (2017) 166–175. https://doi.org/10.1016/j.compositesa.2017.03.033.

[45] O.-K. Park, P.S. Owuor, Y.M. Jaques, D.S. Galvao, N.H. Kim, et al., Hexagonal boron nitride-carbon nanotube hybrid network structure for enhanced thermal, mechanical and electrical properties of polyimide nanocomposites, Compos. Sci. Technol. 188 (2020) 107977. https://doi.org/10.1016/j.compscitech.2019.107977.

[46] W. Yan, Y. Zhang, H. Sun, S. Liu, Z. Chi, et al., Polyimide nanocomposites with boron nitride-coated multi-walled carbon nanotubes for enhanced thermal conductivity and electrical insulation, J. Mater. Chem. A. 2 (2014) 20958–20965. https://doi.org/10.1039/C4TA04663C.

[47] D.P. Kim, C.G. Gofer, J. Economy, Fabrication and properties of ceramic composites with a boron nitride matrix, J. Am. Ceram. Soc. 78 (1995) 1546–1552. https://doi.org/10.1111/j.1151-2916.1995.tb08850.x.

[48] M. Khalaj, S. Zarabi Golkhatmi, S.A.A. Alem, K. Baghchesaraee, M. Hasanzadeh Azar, S. Angizi, Recent progress in the study of thermal properties and tribological behaviors of hexagonal boron nitride-reinforced composites, J. Compos. Sci. 4 (2020) 116. https://doi.org/10.3390/jcs4030116.

[49] A.G. EVans, E.A. Charles, Fracture toughness determinations by indentation, J. Am. Ceram. Soc. 59 (1976) 371–372. https://doi.org/10.1111/j.1151-2916.1976.tb10991.x.